Current Applied Physics 13 (2013) 302–306

Contents lists available at SciVerse ScienceDirect

Current Applied Physics

journal homepage: www.elsevier.com/locate/cap

Improvement of performance of tetraphenylporphyrin-based red organic light emitting diodes using WO_3 and C_{60} buffer layers

Mina Neghabi [a], Abbas Behjat [b,*], Bi Bi Fatemeh Mirjalili [c], Leila Zamani [c]

[a] Department of Physics, Islamic Azad University, Najafabad Branch, Isfahan, Iran
[b] Atomic and Molecular Group, Physics Department, Yazd University, Yazd 89195-741, Iran
[c] Chemistry Department, College of Science, Yazd University, Yazd, Iran

ARTICLE INFO

Article history:
Received 5 October 2011
Received in revised form
24 April 2012
Accepted 7 August 2012
Available online 13 August 2012

Keywords:
Red organic light-emitting diodes
Meso-tetraphenylporphyrin (TPP)
Tungsten oxide (WO_3)
Fullerene (C_{60})
Electroluminescence performance

ABSTRACT

One of the porphyrin derivatives, meso-tetraphenylporphyrin (TPP), has been synthesized and examined as an emitter material (EM) for efficient fluorescent red organic light-emitting diodes (OLEDs). By inserting a tungsten oxide (WO_3) layer into the interface of anode (ITO) and hole transport layer N,N′-Di-[(1-napthyl)-N,N′-diphenyl]-(1,1′-biphenyl)-4,4′-diamine (NPB) and by using fullerene (C_{60}) in contact with a LiF/Al cathode, the performance of devices was markedly improved. The current density–voltage–luminance (J–V–L) characterizations of the samples show that red OLEDs with both WO_3 and C_{60} as buffer layers have a lower driving voltage and higher luminance compared with the devices without buffer layers. The red OLED with the configuration ITO/WO_3 (3 nm)/NPB (50 nm)/TPP (60 nm)/BPhen (30 nm)/C_{60} (5 nm)/LiF (0.8 nm)/Al (100 nm) achieved the high luminance of 6359 cd/m^2 at the low driving voltage of 8 V. At a current density of 20 mA/cm^2, a pure red emission with CIE coordinates of (0.65; 0.35) is observed for this device. Moreover, a power efficiency of 2.07 lm/W and a current efficiency of 5.17 cd/A at 20 mA/cm^2 were obtained for the fabricated devices. The study of the energy level diagram of the devices revealed that the improvement in performance of the devices with buffer layers could be attributed to lowering of carrier-injecting barrier and more balanced charge injection and transport properties.

1. Introduction

Since Tang *et al.* [1] for the first time demonstrated efficient multilayer organic light-emitting diodes (OLEDs) with a significant performance, they have attracted much attention because of their potential applications in large-area low-cost flexible display and solid-state lighting [2,3]. In fluorescent OLEDs, in spite of the synthesis and development of various fluorescent materials such as green, blue and red emitters, little attention has been paid to red fluorescent materials. Red emissive-materials are normally prone to aggregation in the solid state. This is due to dipole–dipole interactions or intermolecular π–π stacking which can lead to an increase in quenching of excitons and a decrease in power efficiency of these materials [4]. One solution to this problem is to dope red-emissive materials into organic host materials [5]. This considerably dilutes the concentration of the emissive dopant and, thus, decreases the aggregation tendency. However, the problem of such doping systems is that the resultant emission color is not pure red because of poor energy transfer processes from the host to the red dopant [6]. This can lead to poor charge carrier transport through the material, which in fact would lead to a decrease in power efficiency. Recently, fabrication of red OLEDs has been reported to be with non-doped red emitters which show a better performance as compared to doping systems [7,8]. Also, fabrication of OLED devices with a high performance and operational stability has been reported through modification of anode/organic and cathode/organic interfaces [9,10]. One of the advantages of modification of electrodes in OLED devices is that can improve the performance of the device remarkably but does not change the emissive color. An improved proposal scheme involves inserting a buffer layer between the anode and the hole transport layer (HTL) [11–14] and inserting a buffer layer into the interface of the electron transport layer (ETL) and the cathode [15,16]. This reduces the charge carrier injection barriers and enhances balancing of the concentrations of charge carriers; this would ultimately enhance the recombination efficiency and improve the performance of the devices.

In this work, we have synthesized a red fluorescent material, meso-tetraphenylporphyrin (TPP), and demonstrated an efficient

* Corresponding author. Tel.: +98 3518122773; fax: +98 351 8200132.
E-mail address: abehjat@yazduni.ac.ir (A. Behjat).

1567-1739/$ – see front matter © 2012 Elsevier B.V. All rights reserved.
http://dx.doi.org/10.1016/j.cap.2012.08.003

non-doped red OLED based on this material. Buffer layers including WO_3 and C_{60} were used in order to study the hole–electron injection effects, improvement in power efficiency and operational stability of the devices.

2. Experimental procedure

2.1. Materials and preparation of meso-tetraphenylporphyrin (TPP)

N,N′-Di-[(1-napthyl)-N,N′-diphenyl]-(1,1′-biphenyl)-4,4′-diamine (NPB), tris (8-hydroxyquinoline) aluminum (Alq_3), 4-7-diphenyl-1,1′-phenanlhroline (BPhen) and buffer materials were purchased from Aldrich Chemical Co. and used as received. The red-emissive TPP was synthesized through the following procedures: pyrrole (3 mmol), benzaldehyde (3 mmol), $ZnCl_2{\cdot}6H_2O$ (0.3 g), silica sulfuric acid (SSA) (0.15 g) and dichloromethane (20 mL) were placed in a 100-mL beaker. The mixture was stirred at room temperature for 2 h. The progress of the reaction was followed by TLC. After 2 h, maximum amounts of tetraphenylporphyrin as the initial product were obtained. Then, 0.3 g of dicyano-dichloro-quinoline (DDQ) and 0.2 g of SSA were added to the mixture and stirred at room temperature for 10 min to oxidize the tetraphenylporphyrinogen into tetraphenylporphyrin. Evaporation of the solvent, and sequential washing of the obtained crude solid with diethyl ether, hot water, and cold methanol, was the method applied for the purification of tetraphenylporphyrine (TPP) as a purple solid with a yield of 50% and m.p. = 300 °C. The spectroscopic data of TPP are as below: UV (CH_2Cl_2), λ_{max} (nm) (log ε): 418 (4.5), 517 (4), 549 (3.84), 591 (3.73), 647 (3.4); FT-IR (KBr) ν: 3311, 3053, 1595, 1469, 1440, 965, 792, 726, 696 cm^{-1}; ^1H NMR ($CDCl_3$, 400 MHz), δ = (ppm): −3 (s, 2H), 7.73 (m, 12H), 8.21 (d, 8H), 8.80 (s, 8H). Scheme 1 shows the synthesis of TPP:

2.2. OLEDs fabrication

Prior to fabricating the OLED devices, ITO-coated glasses with a sheet resistance of 15 Ω/sq were cleaned sequentially by ultrasonication in deionized water, acetone, methanol, isopropyl alcohol for 15 min. Finally, the substrates were blown dry with high-purity N_2 gas stream before they were loaded into a vacuum chamber for nano-layer film deposition. In our work, the configurations of the red OLED devices are as follows:

Device 1: ITO/NPB (50 nm)/TPP (60 nm)/Alq_3 (30 nm)/LiF (0.8 nm)/Al (150 nm).

Device 2: ITO/NPB (50 nm)/TPP (60 nm)/BPhen (30 nm)/LiF (0.8 nm)/Al (150 nm).

Device 3: ITO/WO_3 (3 nm)/NPB (50 nm)/TPP (60 nm)/Alq_3 (30 nm)/LiF (0.8 nm)/Al (150 nm).

Device 4: ITO/WO_3 (3 nm)/NPB (50 nm)/TPP (60 nm)/BPhen (30 nm)/LiF (0.8 nm)/Al (150 nm).

Device 5: ITO/WO_3 (3 nm)/NPB (50 nm)/TPP (60 nm)/Alq_3 (30 nm)/C_{60} (5 nm)/LiF (0.8 nm)/Al (150 nm).

Device 6: ITO/WO_3 (3 nm)/NPB (50 nm)/TPP (60 nm)/BPhen (30 nm)/C_{60} (5 nm)/LiF (0.8 nm)/Al (150 nm).

Here, NPB and TPP were used as hole-transport and emissive layers, and BPhen and Alq_3 as electron-transport layers respectively. All the layers (organic layers, buffer layers and aluminum electrode) of the OLED devices were fabricated by thermal evaporation without breaking the vacuum. The vacuum chamber pressure was kept below 3×10^{-5} mbar. All the organic materials were deposited at a deposition rate of 0.2–0.4 nm/s and the buffer layers were deposited on ITO anode at a rate of 0.01 nm/s. The deposition rate was maintained at 0.01 nm/s for LiF and 0.6–1 nm/s for the aluminum cathode. The emitting area was 0.3×0.5 cm^2.

The electroluminescence characteristics of the devices including the electroluminescence (EL) spectra, current density–voltage (J–V) and luminance characteristics were measured using Keithley 2400 source-meter and a Jaz spectrometer (Ocean optics). All the electroluminescence characteristics were achieved at room temperature and under ambient conditions without any encapsulation.

3. Results and discussion

Fig. 1(a) and (b) depicts the current density versus voltage (J–V) and the luminance versus voltage (L–V) graphs for the OLED devices D1, D2, D3, D4, D5 and D6. As it can be seen, the driving voltage of the devices containing WO_3 and C_{60} as buffer layers (D3, D4, D5 and D6) is lower than that of the devices without buffer layers (D1 and D2). In particular, at the same current density of 20 mA/cm^2, the device D6 (with two buffer layers and with BPhen as ETL layer) has the lowest driving voltage 3.5 V compared with the other devices. That is to say, the driving voltages are 7.8, 7.3, 6.9, 6.8 and 5.5 V for D1, D2, D3, D4 and D5 respectively. On the other hand, a dramatic increase in the current density is observed at the same operating voltage for the devices with two buffer layers (D5 and D6) in comparison to the other four devices (D1, D2, D3 and D4). It is clear that the slope of I–V curve and that of the luminance–bias voltage curve of device D6 is larger than those of the others at a bias voltage above 5 V. So, device 6 shows a higher luminance among the devices. For instance, the luminance of 6359 cd/m^2, at a bias voltage of 8 V is obtained for D6, while the luminance of D1, D2, D3, D4 and D5 reach 103.6, 179.5, 879.3, 1947 and 3681 cd/m^2 respectively, at the same voltage. Therefore, the devices with buffer layers show significant improvement in the luminance performance of red OLEDs in comparison with those without a buffer layer. The results agree with other reports [17–21]. By considering the energy level diagram of the studied devices, as shown in Fig. 2(a) and (b), it is seen that when WO_3 is used as a buffer layer at the ITO and NPB interface, a significant interface dipole forms on ITO, thus leading to the increase of ITO work

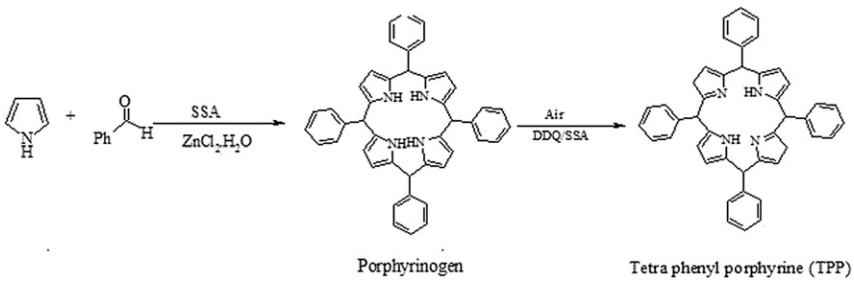

Scheme 1. Synthesis of the meso-tetraphenylporphyrin (TPP).

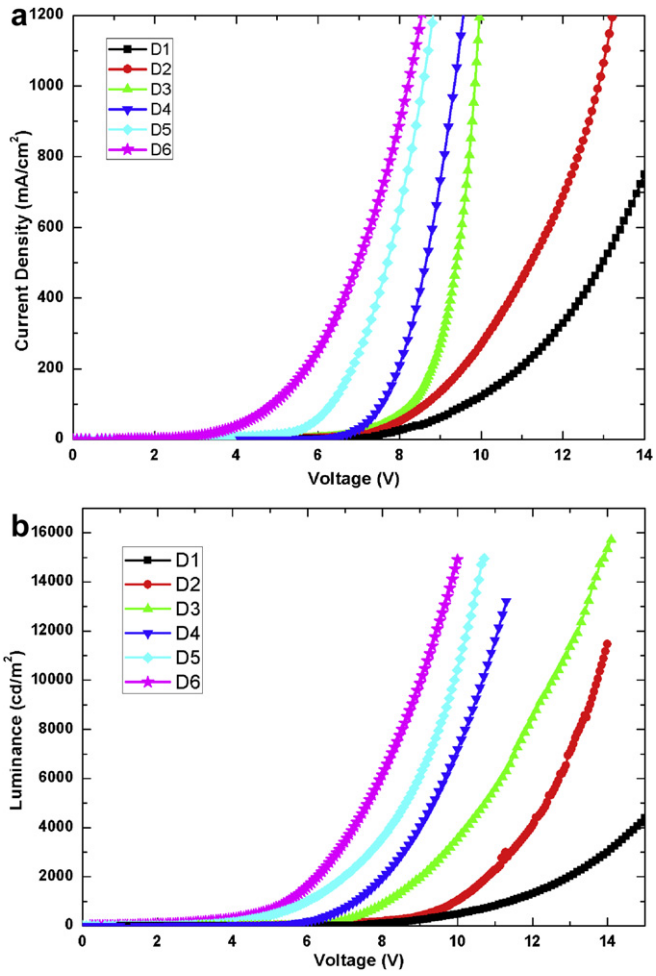

Fig. 1. (a) Current density–voltage and (b) luminance–voltage characteristics of the devices with configurations of D1, D2, D3, D4, D5 and D6, respectively.

function. Beside an additional dipole layer forms between NPB and WO_3 because WO_3 draws charge from the NPB due to strong electron donating property of NPB. Therefore by inserting WO_3 the hole injection barrier decreases and hole injection enhancement is observed. In fact, according to the Fowler–Nordheim (F–N) field emission tunneling theory, these results indicate that the tunneling of holes between anode and HTL is easier due to a potential drop across WO_3 buffer layer, and an ohmic contact is formed at the anode–HTL interface. As a result, the driving voltage is reduced and the overall current density and the luminance of OLEDs are increased. Moreover, the decrease of driving voltage and the enhancement of luminance for the devices with C_{60} as a buffer layer (D5 and D6) are due to the strong electron-accepting ability of C_{60}. It is reported that C_{60} with extended surface orbitals and a low LUMO energy level has a highly conductive electron-transport characteristic in contact with a LiF/Al cathode [22]. Also, the considerable electroluminescence (EL) performances of D6 compared with D5 are attributed to the better electron injection and transport of the electrons from the electrode to the emission zone. This is due to the higher electron mobility of BPhen compared to Alq_3. It is reported that the electron mobility of BPhen is about 200 times more than that of Alq_3 [23]. Thus, it is expected that the use of WO_3 and C_{60} as buffer layers at the ITO–NPB interface and BPhen–LiF interface can have a significant effect on EL performances of the OLEDs.

In order to investigate the device's operational stability, the plots of the current efficiency and power efficiency as a function of the current density are shown in Fig. 3(a) and (b). It can be seen that the power efficiency indexes of devices D3, D4, D5 and D6 are all larger than those of D1 and D2 at the same current density. Since the power efficiency depends on the charge injection barriers and the driving voltage of the device, at a current density of 20 mA/cm^2, a power efficiency of 2.07 lm/W is obtained for the device with structure ITO/WO_3 (5 nm)/NPB (50 nm)/TPP (60 nm)/BPhen (30 nm)/C_{60} (5 nm)/LiF (0.8 nm)/Al (150 nm) (D6) with the lowest driving voltage which is increased by about ≈32%, compared to all the other devices. However, it is found that the current efficiency of the devices with one buffer layer (D3 and D4) is lower than those without a buffer layer (D1 and D2); this is due to unbalanced charge injection and transport, which ultimately limits the current efficiency. In fact, as demonstrated, when WO_3 is used as a buffer layer, the hole injection is much larger than the electron injection for D3 and D4. Thus, this suggests that the carrier injection and transport are unbalanced and the holes are the dominant charge carriers which lead to a lower current efficiency. It is well known that a higher current efficiency of an organic device will lead to a lower quenching of excitons in an emission zone, which in turn leads to higher device operational stability. When C_{60} is inserted at the ETL–cathode interface of devices D5 and D6, the balance of electron and hole currents improves and, hence, the current efficiency and stability of the devices are enhanced.

For more investigation of the effect of WO_3 and C_{60} layers on the improvement of the power efficiency of the OLEDs, a series of electron-only and hole-only devices are prepared. These devices have the following structures:

DH1: ITO/NPB (50 nm)/LiF (0.8 nm)/Al (150 nm).
DH2: ITO/WO_3 (3 nm)/NPB (50 nm)/LiF (0.8 nm)/Al (150 nm).
DE1: ITO/Alq_3 (30 nm)/LiF (0.8 nm)/Al (150 nm).
DE2: ITO/Alq_3 (30 nm)/C_{60} (5 nm)/LiF (0.8 nm)/Al (150 nm).
DE3: ITO/BPhen (30 nm)/LiF (0.8 nm)/Al (150 nm).
DE4: ITO/BPhen (30 nm)/C_{60} (5 nm)/LiF (0.8 nm)/Al (150 nm).

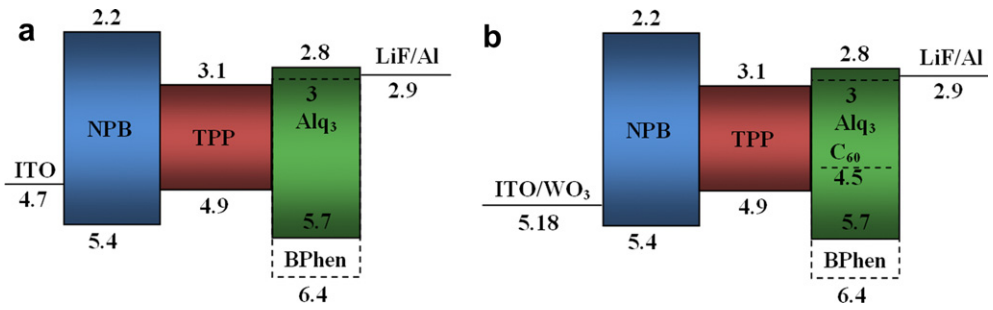

Fig. 2. Schematic illustration of energy level diagram of the devices (a) without any buffer layer and (b) with WO_3 and C_{60} as buffer layers.

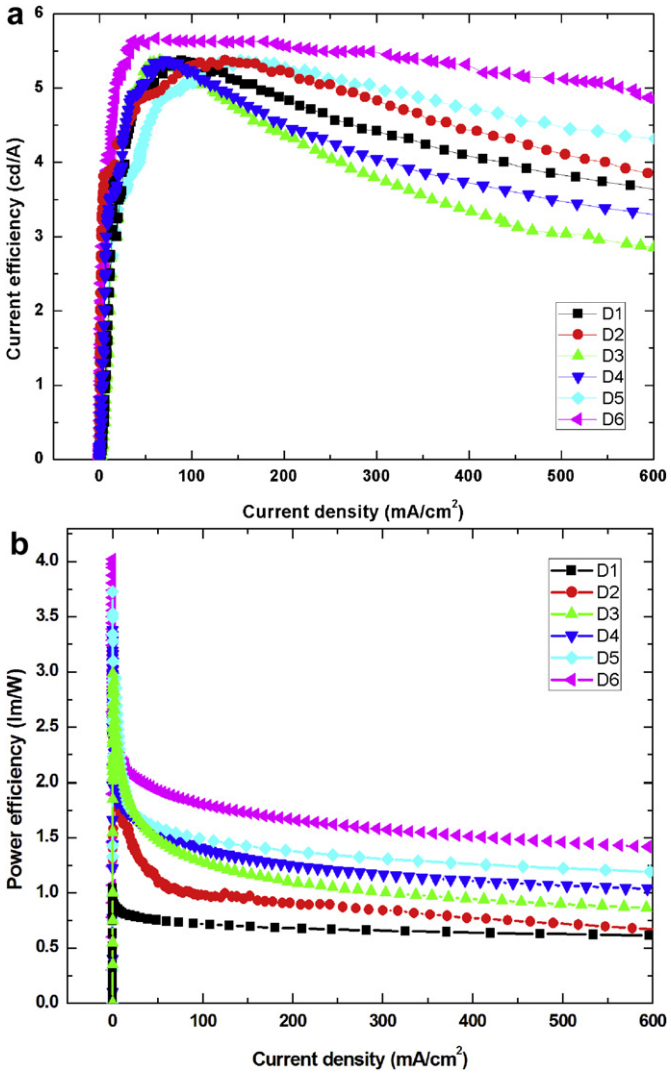

Fig. 3. (a) Current efficiency–current density and (b) power efficiency–current density characteristics of the devices with configurations of D1, D2, D3, D4, D5 and D6 respectively.

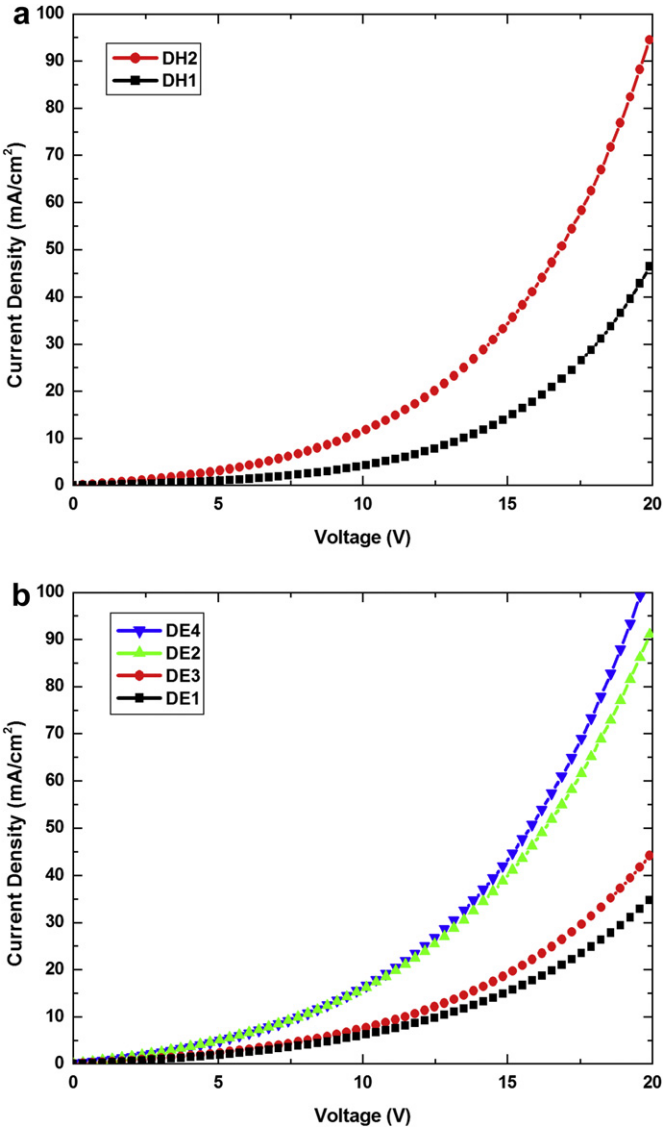

Fig. 4. (a) Current density versus voltage characteristics of the hole-only devices. (b) Current density versus voltage characteristics of the electron-only devices.

The current density–voltage characteristics of electron-only and hole-only devices are shown in Fig. 4(a) and (b). For hole-only devices, the driving voltage of device DH1 was shifted to a higher voltage than that of device DH2 in order to obtain the same current injection. In fact, there is a possibility that the insertion of the WO_3 layer at the ITO–NPB interface improved the hole injection, resulting in a low driving voltage. For electron-only devices, the devices with a 5-nm-thick C_{60} layer in contact with LiF/Al cathode (DE2 and DE4) exhibited a higher current density (17 mA/cm^2) than (7 mA/cm^2) compared with the devices without C_{60} layer (DE1 and DE3) at the same voltage (10 V). It indicated that the insertion of the C_{60} layer improves the electron injection process. Hence, the power efficiency was improved by the insertion of the WO_3 and C_{60} layers. Also, the current density of device DE3 was lower than that of device DE4 at the same voltage. This may be attributed to the weaker conductibility of Alq_3 than that of BPhen.

Fig. 5(a) and (b) shows the EL spectra of Alq_3 and BPhen-based red emissive OLEDs under the current density of 20 mA/cm^2. For all the devices, two emission peaks at 658 and 697 nm can be observed which have originated from the red emitter TPP. Also, it can be seen that there is a shoulder around 560 nm in D1, D3 and D5, which can be attributed to the green emission of Alq_3. It seems that this shoulder may be either introduced by the exciton diffusion from TPP into Alq_3 or caused by the direct electron–hole recombination inside Alq_3. For the devices with a buffer layer, it may be concluded that the increase in the emission intensity in the EL spectra is due to the improvement in the charge carrier injection and transport and the increase in the probability of electron–hole recombination in OLEDs. Also, because of the better hole-blocking characteristic of BPhen [24], BPhen-based devices (D2, D4 and D6) have a better performance than Alq_3-based devices. At a current density of 20 mA/cm^2, a pure red emission with CIE coordinates of (0.64; 0.35), (0.64; 0.34) and (0.65; 0.35) is observed for BPhen-based devices with D2, D4 and D6 configurations respectively. In comparison, we can observe that CIE coordinate of device D6 becomes better due to the insertion of WO_3 and C_{60} as buffer layers. On the other hand, it can be found that Alq_3-based devices have a low pure red emission because the emission from them is often contaminated by the residual green emission from

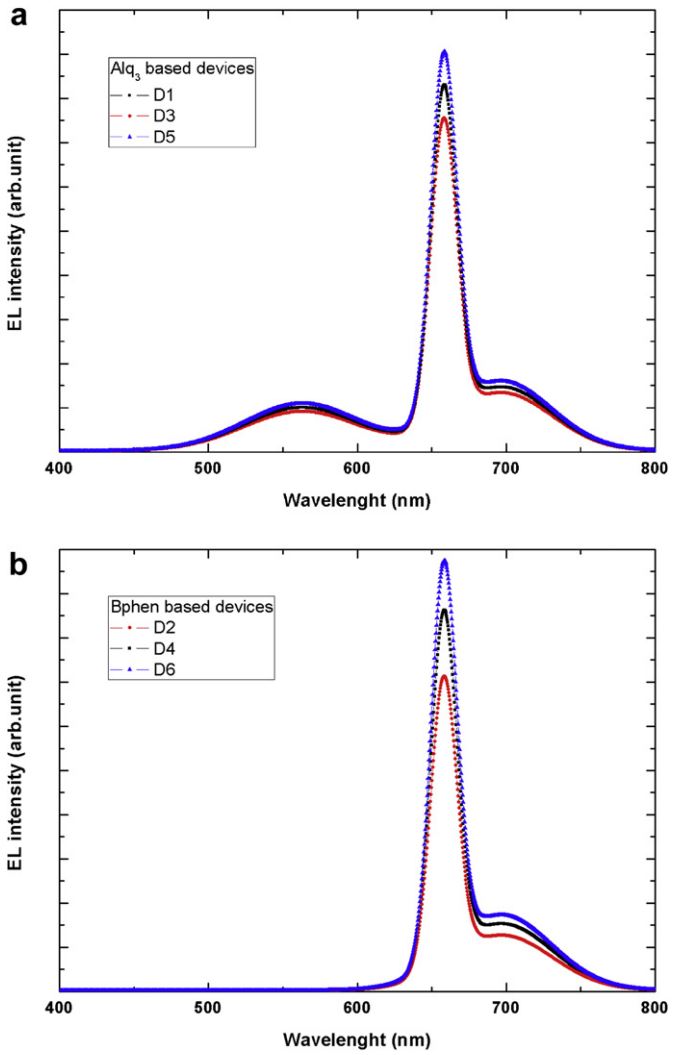

Fig. 5. (a) Normalized EL spectra of Alq_3-based devices at a current density of 20 mA/cm^2. (b) Normalized EL spectra of BPhen-based devices at a current density of 20 mA/cm^2.

Alq_3. Therefore, D1, D3 and D5 devices show CIE coordinates of (0.62; 0.36), (0.61; 0.37) and (0.63; 0.36) respectively.

4. Conclusion

Non-doped red organic light emitting diodes using TPP show improved electroluminescence performances by insertion of WO_3 and C_{60} films as buffer layers into the interface of ITO–HTL and the interface of ETL–cathode respectively. The BPhen based device with two buffer layers of WO_3 and C_{60} reveals an improved power and current efficiencies, 2.07 lm/W and 5.17 cd/A, compared with other devices. High charge carrier injection and transport characteristics and the balance of holes and electrons in this structure account for these improvements. As a result, this type of structure with a high performance and good operational stability is promising for OLEDs device design and various light-emitting applications.

Acknowledgments

The support of the Ministry of Energy for this project is gratefully acknowledged. Authors also wish to thank the Photonics Group of Physics Department, Yazd University for laboratory support.

References

[1] C.W. Tang, S.A. VanSlyke, Appl. Phys. Lett. 51 (1987) 913–915.
[2] J. Feng, T. Okamoto, R. Naraoka, S. Kawata, Appl. Phys. Lett. 93 (2008) 051106–051108.
[3] M. Eritt, C. May, K. Leo, M. Toerker, C. Radehaus, Thin Solid Films 518 (2010) 3042–3045.
[4] Chin-Ti Chen, Chem. Mater. 16 (2004) 4389–4400.
[5] Huiying Fu, Huanrong Wu, Xiaoyuan Hou, Fei Xiao, Bingxian Shao, Curr. Appl. Phys. 7 (2007) 697–701.
[6] C.J. Huang, T.H. Meen, S.L. Wu, C.C. Kang, Displays 30 (2009) 164–169.
[7] H.-C. Yeh, S.-J. Yeh, C.-T. Chen, Chem. Commun. (2003) 2632–2633.
[8] K.R.J. Thomas, J.T. Lin, M. Velusamy, Y.-T. Tao, C.-H. Chuen, Adv. Funct. Mater. 14 (2004) 83–90.
[9] Q. Huang, J. Li, G.A. Evmenenko, P. Dutta, T.J. Marks, Chem. Mater. 18 (2006) 2431–2442.
[10] X. Xu, G. Yu, Y. Liu, D. Zhu, Displays 27 (2006) 24–34.
[11] J. Wu, J. Hou, Y. Cheng, Z. Xie, L. Wang, Semicond. Sci. Technol. 22 (2007) 824–826.
[12] J. Meyer, S. Hamwi, T. Bülow, H.H. Johannes, T. Riedl, W. Kowalsky, Appl. Phys. Lett. 91 (2007) 113506–113508.
[13] H.C. Im, D.C. Choo, T.W. Kim, J.H. Kim, J.H. Seo, Y.K. Kim, Thin Solid Films 515 (2007) 5099–5102.
[14] Z.H. Huang, X.T. Zeng, E.T. Kang, Y.H. Fuhc, L. Lu, Surf. Coat. Technol. 198 (2005) 357–361.
[15] L.S. Hung, C.W. Tang, M.G. Mason, Appl. Phys. Lett. 70 (1997) 152.
[16] W. Ji, L. Zhang, M. Liu, J. Wang, G. Liu, W. Xie, H. Zhang, Curr. Appl. Phys. 11 (2011) 1410–1413.
[17] Y. Zou, Zh. Deng, Zh. Lv, Zh. Chen, D. Xu, Y. Chen, Y. Yin, H. Du, Y. Wang, J. Lumin. 130 (2010) 959–962.
[18] L. Hou, P. Liu, Y. Li, Ch. Wu, Thin Solid Films 517 (2009) 4926–4929.
[19] J. Li, M. Yahiro, K. Ishida, H. Yamada, K. Matsushige, Synth. Met. 151 (2005) 141–146.
[20] J.W. Kwon, J.T. Lim, G.Y. Yeom, Thin Solid Films 518 (2010) 6339–6342.
[21] Sh Shi, D. Ma, Thin Solid Films 518 (2010) 4874–4878.
[22] X.D. Feng, C.J. Huang, V. Lui, R.S. Khangura, Z.H. Lu, Appl. Phys. Lett. 86 (2005) 143511–143513.
[23] M.A. Khan, W. Xu, K.U. Haq, Y. Bai, X.Y. Jiang, Z.L. Zhang, W.Q. Zhu, J. Appl. Phys. 103 (2008) 014509–014512.
[24] M.A. Khan, W. Xu, F. Wei, Y. Bai, X.Y. Jiang, Z.L. Zhang, W.Q. Zhu, Solid State Commun. 144 (2007) 343–346.